Biosensors and Bioelectronics 290 (2025) 118014

Contents lists available at ScienceDirect

Biosensors and Bioelectronics

journal homepage: www.elsevier.com/locate/bios

Dendrimer-based DNA biosensor for HIV virus detection

Estefanía Enebral Romero [a,b], Marta Toldos-Torres [a], David López-Diego [c], Mónica Luna [c], Marta Failde [d], Brais González-Tobío [e], Félix Zamora [e,f], Iker Falces-Romero [g], María Luisa Montes [h], Tania García-Mendiola [a,f,*]

[a] Departamento de Química Analítica y Análisis Instrumental, Universidad Autónoma de Madrid, 28049, Madrid, Spain
[b] IMDEA-Nanociencia, Ciudad Universitaria de Cantoblanco, 28049, Madrid, Spain
[c] Instituto de Micro y Nanotecnología IMN-CNM, CSIC (CEI UAM+CSIC), Isaac Newton 8, Tres Cantos, 28760, Madrid, Spain
[d] Departamento de Biología Molecular, Facultad de Ciencias, Centro de Biología Molecular Severo Ochoa (CBMSO), Universidad Autónoma de Madrid-Consejo Superior de Investigaciones Científicas, 28049, Madrid, Spain
[e] Departamento de Química Inorgánica and Condensed Matter Physics Center (IFIMAC), Universidad Autónoma de Madrid, 28049, Madrid, Spain
[f] Institute for Advanced Research in Chemical Sciences (IAdChem), Universidad Autónoma de Madrid, 28049, Madrid, Spain
[g] Servicio de Microbiología y Parasitología Clínicas, Hospital Universitario La Paz, IdiPaz, CIBERINFEC, 28046, Madrid, Spain
[h] Servicio de Medicina Interna, Unidad de VIH, Hospital Universitario La Paz, IdiPAZ, CIBERINFEC, 28046, Madrid, Spain

ARTICLE INFO

Keywords:
DNA dendrimer
Few-layer bismuthene (FLB)
Azure A (AA)
DNA biosensor
Human immunodeficiency virus (HIV)

ABSTRACT

In this work, we propose an innovative electrochemical DNA biosensor for the early, rapid, selective, and sensitive detection of the human immunodeficiency virus (HIV) based on its genetic code. This platform is based on the integration of few-layer bismuthene (FLB) which provides a nanostructured surface and facilitates the anchoring of the DNA dendrimer which incorporates the biorecognition element (a capture probe complementary to the HIV-specific DNA sequence). The hybridization between the capture probe and the specific HIV target sequence is detected using Azure A (AA) as a redox indicator. The dendrimer-based DNA biosensor selectively detects HIV from 10.0 fM to 10.0 pM, exhibit a low detection limit of 3.03 fM and a 60-day stability, and has been validated using plasma samples from infected patients with varying viral loads.

1. Introduction

The human immunodeficiency virus (HIV), a type of retrovirus that targets the $CD4^+$ cells of the human immune system, compromises the body's ability to combat diseases and infections. HIV is the primary cause of the disease known as acquired immunodeficiency syndrome (AIDS), transmitted through contaminated blood transfer, sexual contact, or from mother to child (Farzin et al., 2020; Rizvi et al., 2023). Although significant advances in diagnosing and treating this disease have been made over the years, through antiretroviral therapies (ART), the number of global HIV infections remains very high, with two-thirds of the total occurring in African regions, where resource capacity and access to detection techniques for a quick and effective diagnosis and treatment of the disease is quite limited. (Kabiibi et al., 2024). Therefore, the scientific community is focusing on finding new methodologies that enable simple, rapid, sensitive, and cost-effective detection of this virus to curb its spread. In this context, electrochemical DNA nanostructured biosensors emerge as an alternative technique due to their robustness, miniaturization capacity, sensitivity, selectivity, portability, ease of use, and low cost.

Due to the numerous advantages presented by electrochemical DNA biosensors, many applications of these devices have been described over the years for the detection of all types of pathogens, such as viruses or bacteria (Abrego-Martinez et al., 2022; Afonso et al., 2013; Liébana et al., 2016; Martínez-Periñán et al., 2021; Qian et al., 2024). However, there is significant ongoing interest in the development of novel biosensing platforms with boosted analytical performance, as the ability to detect low viral loads is critical for accurate disease diagnosis. It has been demonstrated that the integration of nanomaterials in biosensor development enhances the sensitivity and stability of these devices. Currently, numerous studies are focused on the application of new two-dimensional (2D) nanomaterials in biosensor development (Yang et al., 2022). One of the most promising emerging 2D-nanomaterial is bismuthene, a bismuth derivate with excellent electrical and mechanical properties, high electrical conductivity, which improves electron transfer, ensuring rapid and detectable electrochemical signals, a high

* Corresponding author. Departamento de Química Analítica y Análisis Instrumental. Universidad Autónoma de Madrid. 28049, Madrid, Spain.
E-mail address: tania.garcia@uam.es (T. García-Mendiola).

https://doi.org/10.1016/j.bios.2025.118014
Received 11 August 2025; Received in revised form 16 September 2025; Accepted 19 September 2025
Available online 26 September 2025

relative surface area, which favours the immobilization of the bio-recognition element through interaction with thiol groups (-SH) (Gutiérrez-Gálvez et al., 2024; Torres et al., 2022), high chemical and thermal stability, and biocompatibility, giving rise to stable platforms that are scalable to the industry and have real-time applications in biomedicine and clinical diagnostics. (Baig, 2023; Rohaizad et al., 2021; Su et al., 2019).

Recent studies have demonstrated that the use of DNA nanostructures (tetrahedral DNA nanostructures, DNA nanoflowers, or DNA nanotubes) as building blocks results in biosensors with advanced properties. (Bai and Wei, 2019; Enebral-Romero et al., 2024; Ye et al., 2024; Zhao et al., 2021). Among the different DNA nanostructures, DNA dendrimers have attracted the attention of the scientific community. DNA dendrimers were prepared for the first time in 1993. They are formed by three-dimensional hyperbranched DNA assemblies with a shape- and size-controlled, bulky, geometrically symmetrical structure, relative conformational rigidity, and chemical stability. One of the most commonly used methodologies for preparing this type of nanostructure, due to the ease of the process, is the divergent growth from Y-shaped DNA monomers (Liu et al., 2021; Zhou et al., 2014). This process involves the controlled hybridization of different Y-shaped DNA monomers, each composed of three single-stranded DNA sequences that are complementary to one another, forming three Y-shaped double helices. Each of the prepared monomers has a free fragment, known as a sticky end, complementary to the free fragments of the other monomers. With the hybridization of these sticky-ends, the different generations of the dendrimer ($G_0 \rightarrow G_n$) will be formed, from the central core to the outer branches, creating the three-dimensional spherical hyperbranched tree-like nanostructure (Meng et al., 2014; Mohri et al., 2012, 2015). Thanks to the potential functionalization of these nanostructures, the outer branches of the DNA dendrimer can be modified with different DNA probe sequences, enabling the detection of a broad spectrum of analytes. In this study, we present the synthesis of a DNA dendrimer incorporating the specific probe sequence designed for HIV detection, referred to as the HIV-based DNA dendrimer ($Dend_{VIH}$-SH). These probe sequences are also thiolated at the 5′-end, allowing the DNA dendrimer to be anchored onto the FLB-nanostructured electrode surface. The use of DNA dendrimers in the development of DNA electrochemical biosensors helps amplify the reporter signal at the working electrode, resulting in a higher hybridization capacity and improved recognition of the hybridization event, which achieves lower detection limits (Xu et al., 2025). This provides biosensors with improved sensitivity and selectivity, making them a potential alternative to traditional detection methods for virus detection (Tian et al., 2024).

Based on the principles outlined above, this work proposes the design and synthesis of a novel DNA dendrimer carrying the specific HIV capture probe (HIV-based DNA dendrimer). An innovative electrochemical DNA biosensor is developed with the immobilization of the DNA dendrimer onto the few-layer bismuthene (FLB) nanostructured electrode surface. Azure A (AA) is employed as a redox indicator of the hybridization event, for the rapid, selective and sensitive detection of the HIV by its genetic code.

2. Material and methods

All the reagents, apparatus and procedures are presented in detail in the Supporting Information.

3. Results

The dendrimer-based DNA biosensor proposed in this work was developed according to the steps outlined in Scheme 1A. The first step involves the nanostructuration of a carbon screen-printed electrode (CSPE) with the FLB through drop casting, facilitated by the interaction between the carbon of the CSPE and the bismuth of the bismuthene (CSPE/FLB). The next step involves the immobilization of the HIV-based DNA dendrimer synthesized (DendVIH-SH probe), resulting from the binding between the thiol group of the $Dend_{VIH}$-SH probe and the bismuth of the bismuthene (CSPE/FLB/$Dend_{VIH}$-SH). Thus, the FLB serves as a nanomaterial for improving the analytical properties of the biosensor and as an anchoring platform for immobilizing the bio-recognition element, the HIV-based DNA dendrimer. Then, the resulting biosensing platform (CSPE/FLB/$Dend_{VIH}$-SH) is faced to the analyte, the HIV-specific DNA sequence, under optimal conditions (40 °C, 1 h, humidity chamber, stirring). The hybridization event is electrochemically detected using Azure A, which act as an electrochemical indicator (CSPE/FLB/$Dend_{VIH}$-SH/HIVc/AA), and differential pulse voltammetry (DPV) as detection technique, in 0.1M PB pH 7.0 electrolyte buffer. All the experimental details are described in the experimental section in the SI.

3.1. HIV-based DNA dendrimer synthesis and characterization

The synthesis of the HIV-based DNA dendrimer follows a divergent-growth strategy from Y-shaped DNA monomers (Y_A, Y_B, and Y_C) through the hybridization of the complementary nitrogenous bases. Y_A (red Y DNA monomer) and Y_B (blue Y DNA monomer) are composed of three 40-base DNA sequences each (TriX-1, TriX-2 and TriX-3), while Y_C includes two 61-base (TriC-1 and TriC-2) and one 40-base DNA sequence. Each monomer contains 12-base sticky-end fragments at the 5′-end, enabling sequential hybridization and the stepwise formation of the dendrimer generations (G_0 to G_2). The TriC-1 and TriC-2 sequences contain two 5′-thiolated 24-base sequences that correspond to the specific HIV probe sequence (yellow sequences), which remain free and available for the hybridization reaction with the target analyte. All sequences are listed and highlighted in different colours in Table S1 of SI and shown in Scheme 1B. Monomers were assembled by mixing equimolar amounts (1.00 μM) of each strand in TE buffer, and dendrimer formation was achieved by mixing Y_A, Y_B, and Y_C in a 1:3:6 ratio. Hybridizations were performed in a thermocycler using temperature-controlled steps, with melting temperatures (T_m) calculated to prevent non-specific binding. All details regarding the synthesis of each monomer and the complete structure of the HIV-based DNA dendrimer are provided in the Experimental and Results sections of the Supporting Information.

Once the HIV-based DNA dendrimer was synthesized under the required experimental conditions, it was verified that the synthesis had been successfully performed using characterization techniques such as electrophoresis, atomic force microscopy (AFM), and scanning electron microscopy with energy dispersive X-ray spectroscopy (SEM-EDX).

The image obtained from the electrophoresis (Fig. 1A) reveals differences between each stage in the formation of the HIV-based DNA dendrimer, resulting from the variations in the weights of the structures. It can be observed that in well 8, where the complete HIV-based DNA dendrimer is located (G_2), the band has moved much slower compared to wells 5, 6 and 7, which contain the different generations and possible combinations between the Y-shaped DNA monomers (G_0, G_1 and Y_B:Y_C, respectively). Similarly, in wells 2, 3, and 4, where the Y_A, Y_B, and Y_C monomers are located, the bands have moved faster due to their lower molecular weights. The bands observed that do not correspond to the marked structures are likely due to fragments that may be, have remained unhybridized or impurities.

Fig. 1 shows the SEM images (Fig. 1B, C, 1F, and 1G) and AFM images (Fig. 1D and H) acquired before (Fig. 1B–D) and after (Fig. 1F–H) the dendrimer immobilization on a silicon substrate modified with evaporated gold. The AFM (Fig. 1D) and SEM (Fig. 1B) images illustrate the characteristic surface morphology of Au, composed of gold grains. In contrast, Fig. 1F and H reveal the presence of dendrimer on the surface, where its well-defined structure can be clearly distinguished. Additionally, the backscattered electron (BSE) images (Fig. 1C and G) highlight contrast differences corresponding to distinct materials. Regions with higher atomic number elements appear brighter, which in this case

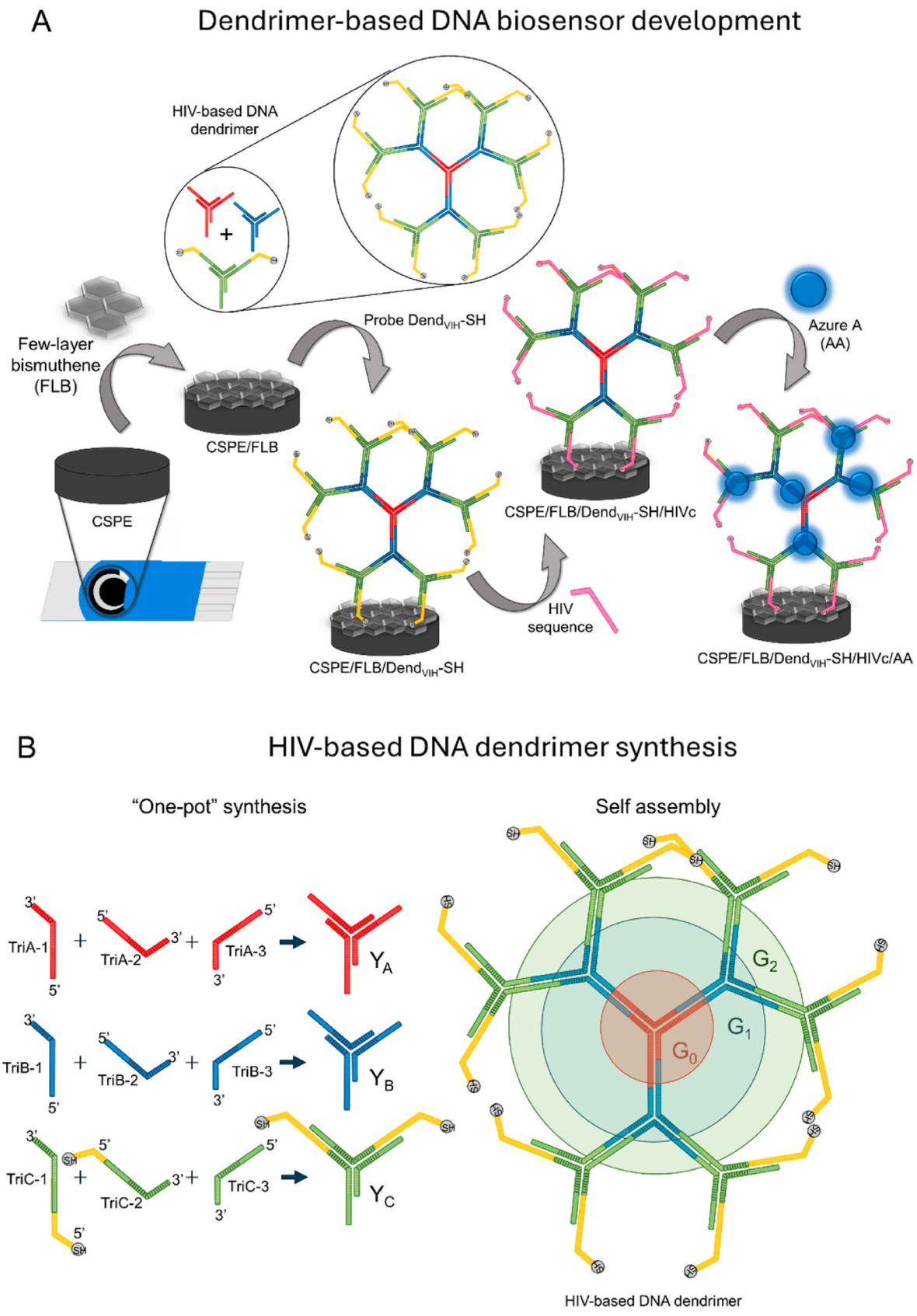

Scheme 1. Scheme of the dendrimer-based DNA biosensor development (**A**) and of the synthesis of the HIV-based DNA dendrimer (**B**).

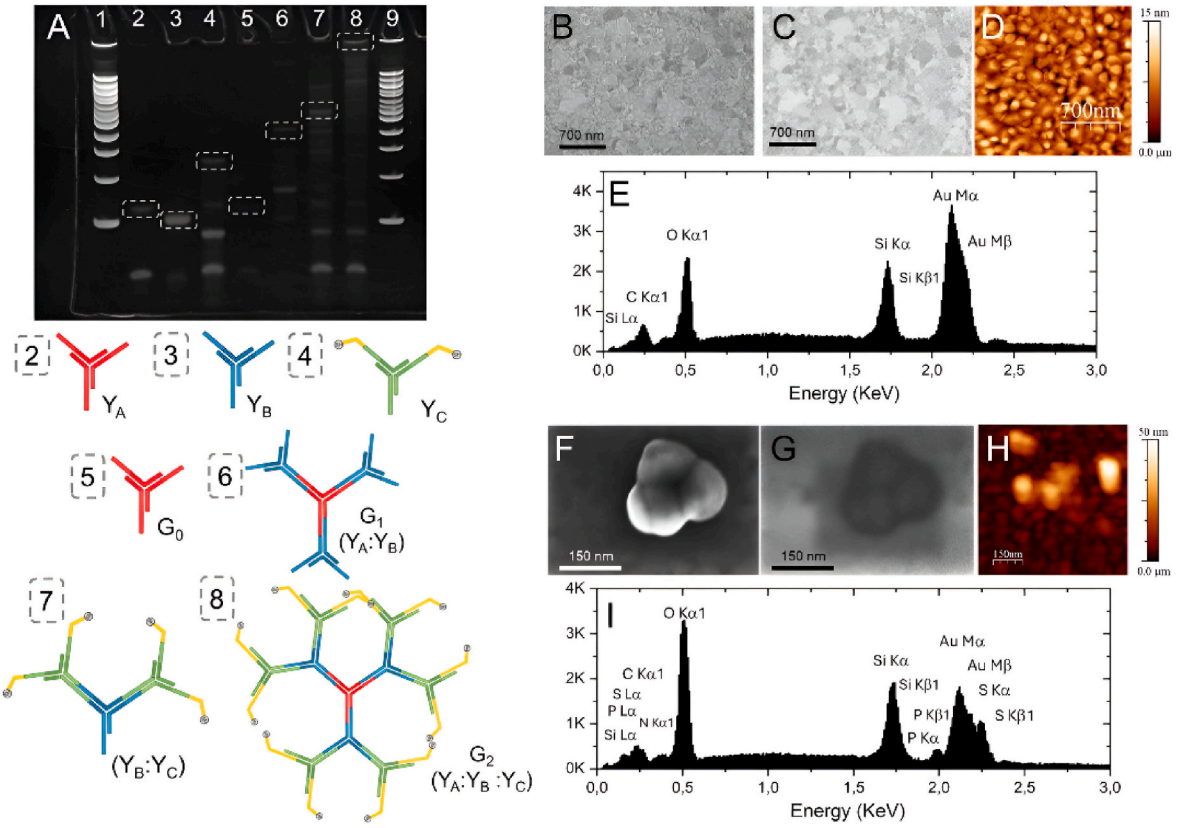

Fig. 1. Gel electrophoresis analysis and schematic representation (**A**) of the different samples studied in the HIV-based DNA dendrimer ($Dend_{VIH}$-SH) synthesis: wells 2 to 4 are the Y-shaped DNA monomers (Y_A, Y_B and Y_C, respectively); wells 5 to 7 are the different dendrimer generations and possible combinations between the monomers (G_0, G_1 and Y_B:Y_C, respectively); well 8 is the complete $Dend_{VIH}$-SH. Images of secondary electrons (SEM) (**B** and **F**), Backscattered electrons images (**C** and **G**), AFM (**D** and **H**) and EDX (**E** and **I**) of silicon substrate modified with evaporated gold (**B-E**) and a silicon substrate modified with evaporated gold and with the $Dend_{VIH}$-SH immobilized (**F-I**). (For interpretation of the references to colour in this figure legend, the reader is referred to the Web version of this article.)

corresponds to gold.

The elemental analysis by energy-dispersive X-ray spectroscopy (EDX) (Fig. 1E and I) of a gold substrate exhibits the characteristic peaks of Au and Si (Fig. 1E). However, after dendrimer immobilization, new peaks associated with the main molecular chain such as N and P appear (Fig. 1I), confirming its successful attachment to the substrate.

3.2. Dendrimer-based DNA biosensor development

As previously described, the dendrimer-based DNA biosensor was developed using the procedure outlined in Scheme 1A. To confirm that all the steps in the development of the dendrimer-based DNA biosensor were correctly performed, various microscopic and spectroscopic techniques, including SEM-EDX, AFM, fluorescence microscopy, Raman spectroscopy, and electrochemical impedance spectroscopy (EIS), were employed.

Fig. 2 presents the SEM (Fig. 2A, B, 2E, 2F, 2I, and 2J) and AFM (Fig. 2C, G, and 2K) images of all the steps involved in the development of the dendrimer-based DNA biosensor. AFM images reveal how the electrode surface morphology changes with each modification step. After nanostructuration of the CSPE electrode with FLB (CSPE/FLB, Fig. 2G), the smooth and homogeneous surface observed on the bare CSPE (Fig. 2C) disappears due to the deposition of bismuthene nanosheets. Upon immobilization of the HIV-based DNA dendrimer ($Dend_{VIH}$-SH) on the CSPE/FLB platform (CSPE/FLB/$Dend_{VIH}$-SH, Fig. 2K), the surface becomes rougher, indicating successful dendrimer attachment. In the SEM image of the unmodified CSPE (Fig. 2A), as it was expected an uniform surface composed of carbon is observed. After the modification and nanostructuration of the CSPE with FLB (CSPE/FLB, Fig. 2E), hexagonal shapes corresponding to the bismuthene nanosheets become visible in the image. Following the immobilization of the $Dend_{VIH}$-SH dendrimer onto the CSPE/FLB platform (CSPE/FLB/$Dend_{VIH}$-SH, Fig. 2I), small spots appear on the bismuthene hexagons, likely corresponding to the spherical nanostructured dendrimer. The backscattered electron image of the bare CSPE (Fig. 2B) lacks contrast, as it presents a homogeneous surface composed solely of carbon. Following modification with FLB (Fig. 2F), lighter areas appear, associated with bismuthene nanosheets, which have a higher atomic number than carbon. For the CSPE/FLB/$Dend_{VIH}$-SH biosensing platform (Fig. 2J), new darker regions are visible on the bismuthene nanosheets, attributed to the immobilized HIV-based DNA dendrimer, which effectively reduces the effective atomic number of the platform.

These results have been confirmed through elemental characterization by energy-dispersive X-ray spectroscopy (EDX). The EDX spectrum of the bare CSPE (Fig. 2D) exhibits the characteristic C peak from the carbon electrode surface. After nanostructuration with FLB (Fig. 2H), additional Bi peaks corresponding to the FLB nanosheets appear. Finally, with the immobilization of the $Dend_{VIH}$-SH dendrimer (Fig. 2L), in addition to the C and Bi peaks, new P peaks corresponding to the phosphate backbone of the HIV-based DNA dendrimer are observed.

Additional complementary characterization studies were also carried out using fluorescence microscopy, Raman spectroscopy, and EIS (Fig. S3, which are discussed in detail in Section 3.3 of the Supporting Information).

The comprehensive analysis performed using multiple characterization techniques confirms the successful performance of each step involved in the development of dendrimer-based DNA biosensors.

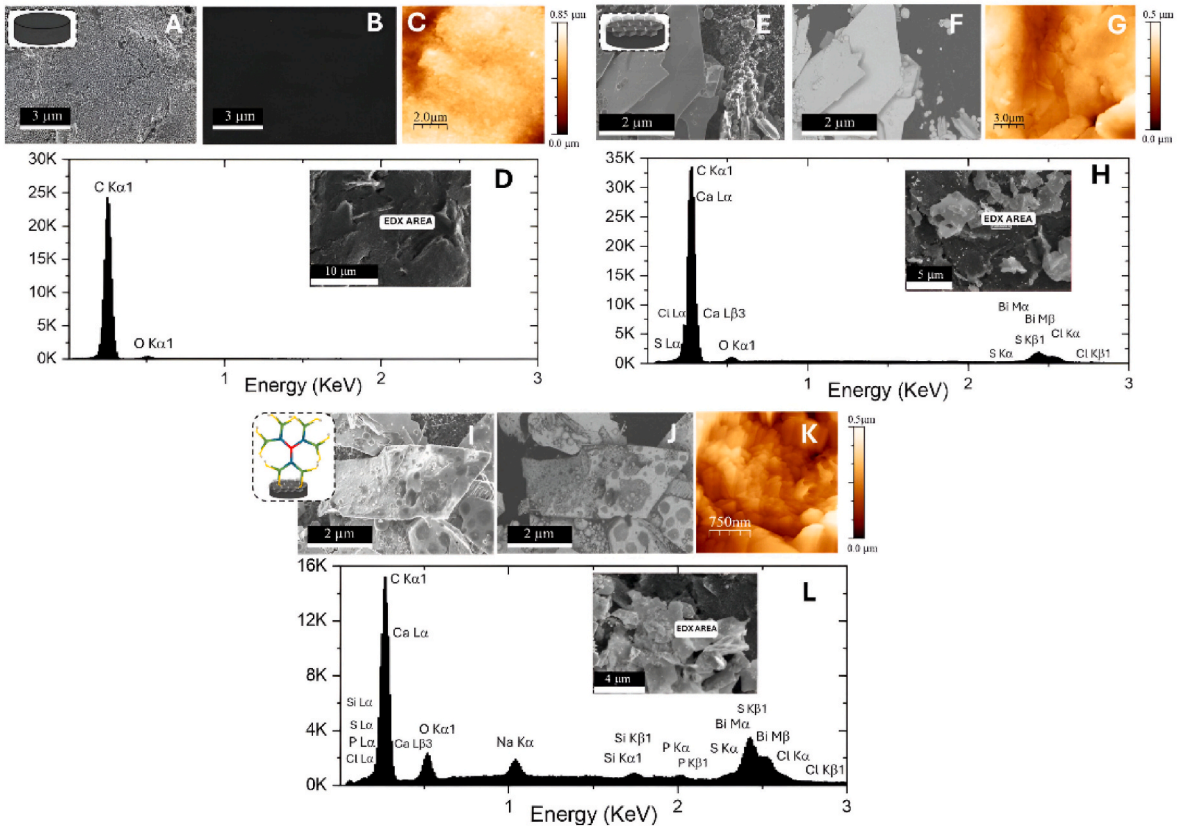

Fig. 2. Secondary electrons images (SEM) (**A**, **E** and **I**), Backscattered electrons images (**B**, **F** and **J**), AFM (**C**, **G** and **K**) and EDX (**D**, **H** and **L**) of a bare CSPE (**A**–**D**), a CSPE modified with FLB (CSPE/FLB, **E**-**H**) and of the DendVIH-SH dendrimer immobilized on the CSPE/FLB platform (CSPE/FLB/DendVIH-SH, **I**-**L**).

3.3. HIV DNA sequence detection

The dendrimer-based DNA biosensor developed was tested for the detection of the HIV virus by its genetic code using differential pulse voltammetry (DPV) as a detection technique. To improve the analytical performance of the device and ensure reproducible results, all steps in the development of the dendrimer-based DNA biosensor were carefully optimized. First, the immobilization time of the HIV-based DNA dendrimer on the electrode (24 h, 1 h, and 30 min) and secondly, its concentration (1.00 µM, 1:2 dilution, and 1:4 dilution) were optimized by comparing the electrochemical response obtained before (CSPE/FLB/$Dend_{VIH}$-SH) and after hybridization with the HIV target sequence (CSPE/FLB/$Dend_{VIH}$-SH/HIVc). For the $Dend_{VIH}$-SH immobilization time optimization, 10.0 µL of the synthesized $Dend_{VIH}$-SH at a concentration of 1.00 µM was immobilized on the CSPE/FLB platform and incubated at room temperature for 24 h, 1 h, or 30 min. After incubation, hybridization with the HIVc sequence at a concentration of 10.0 fM was performed under optimal conditions (40 °C, 1 h, in a humidity chamber, with mechanical agitation). Finally, the platform was incubated with Azure A (at room temperature, 1 h, in the dark), and the DPV was recorded using 0.1M PB pH 7.0 buffer as electrolyte. Fig. 3A presents the relative reduction in current intensity observed before and after the hybridization process, as a function of the different incubation times applied for $Dend_{VIH}$-SH. As shown, the highest percentage signal decrease is obtained for a 1-h incubation time, making it the selected optimal time for dendrimer-based DNA biosensor development. On the other hand, for the optimization of HIV-based DNA dendrimer concentration, 10.0 µL of $Dend_{VIH}$-SH at a concentration of 1.00 µM, diluted 1:2 and 1:4, was incubated on the CSPE/FLB platform for 1 h. After the hybridization with HIVc 100 pM and incubation with Azure A, the current intensities depicted in Fig. 3B were obtained for each concentration. It is observed that in the case of 1.00 µM $Dend_{VIH}$-SH, there is a significantly higher decrease in current intensity and better reproducibility after the hybridization event, compared to the other cases. Therefore, this is the selected optimal concentration.

Once the steps in the dendrimer-based DNA biosensor development were optimized, its sensitivity and selectivity for HIV were evaluated. Fig. 3C shows the DPVs obtained for the oxidation of Azure A at −0.45V, for the dendrimer-based DNA biosensor in absence (CSPE/FLB/$Dend_{VIH}$-SH, black line) or in presence of the HIV sequence (CSPE/FLB/$Dend_{VIH}$-SH/HIVc, red line) or a non-complementary sequence (CSPE/FLB/$Dend_{VIH}$-SH/NC, blue line) at a concentration of 100 pM. As illustrated, only when the biosensing platform is faced to the specific HIV sequence (HIVc), a decrease in the anodic current intensity is observed compared to the blank (prior to hybridization), due to the hybridization between the capture sequence integrated into the DNA dendrimer structure ($Dend_{VIH}$-SH) and the HIVc These results confirm the ability of the biosensor to selectively recognize the HIV-specific genetic code.

To confirm the sensitivity improvements provided by the use of dendrimers in the field of sensing, the biosensor response was compared using either a DNA probe (HIV-SH) or the synthesized HIV-based DNA dendrimer ($Dend_{VIH}$-SH) as the biorecognition element.

Over the years, it has been demonstrated that the arrangement of the DNA probe on the electrode surface affects the hybridization event. It is essential for the DNA probe to be well-oriented and evenly spaced across the electrode surface to facilitate efficient hybridization with the specific analyte DNA sequence. Numerous studies state that the duration of DNA probe immobilization on the electrode surface plays a critical role in the successful fabrication and performance of biosensors. Therefore, in this work, a DNA biosensor was prepared, using a thiolated-DNA capture probe complementary to the HIV (HIV-SH) as biorecognition element, and different immobilization times of the DNA capture probe (1, 24, and 72 h) were tested to determine which time shows the greatest signal difference before (CSPE/FLB/HIV-SH) and after hybridization with the

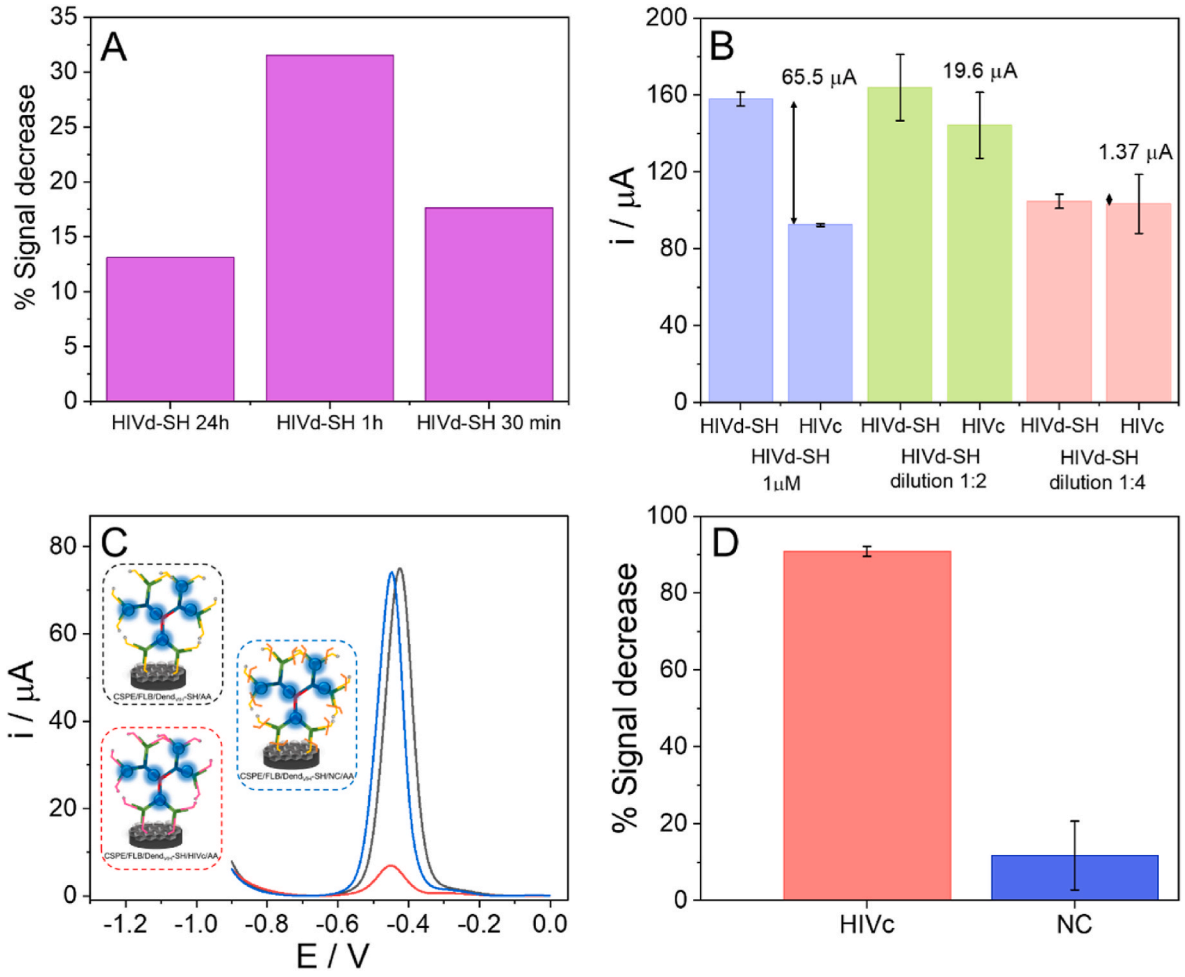

Fig. 3. Column chart illustrating the percentage decrease in electrochemical signal of the CSPE/FLB/Dend$_{VIH}$-SH biosensing platform after hybridization with the HIVc sequence at 10.0 fM concentration for different HIV-based DNA dendrimer incubation times (**A**). Comparative column chart of the current intensity recorded before (CSPE/FLB/Dend$_{VIH}$-SH) and after hybridization with 100 pM HIVc (CSPE/FLB/Dend$_{VIH}$-SH/HIVc), across different concentrations of Dend$_{VIH}$-SH (**B**). Differential Pulse Voltammogram (DPV) of the Azure A oxidation at −0.45 V obtained prior to hybridization (CSPE/FLB/Dend$_{VIH}$-SH, black line), following incubation with HIV DNA sequence (CSPE/FLB/Dend$_{VIH}$-SH/HIVc, red line), and with a non-complementary sequence (CSPE/FLB/Dend$_{VIH}$-SH/NC, blue line), each at a 100 pM concentration (**C**). Column chart of the percentage electrochemical signal decrease obtained for the CPSE/FLB/Dend$_{VIH}$-SH platform after the hybridization with the specific HIV DNA sequence (HIVc, red bar) or a non-complementary sequence (NC, blue bar) (**D**). (For interpretation of the references to colour in this figure legend, the reader is referred to the Web version of this article.)

specific HIV sequence (CSPE/FLB/HIV-SH/HIVc). To evaluate the selectivity of the biosensor, the platform was exposed to a non-complementary sequence (CSPE/FLB/HIV-SH/NC).

Fig. S4 shows the percentage decrease in the electrochemical signal recorded for the oxidation of Azure A at −0.45V, obtained for the CSPE/FLB/HIV-SH platform at different DNA probe immobilization times (1 h, purple bar; 24 h, orange bar and 72 h, blue bar) after facing the platform to the HIV specific sequence (HIVc) or to a non-complementary sequence (NC) at a concentration of 100 pM. As evidenced by the results, all cases exhibit a more pronounced signal reduction following incubation with the HIV complementary sequence (HIVc) compared to the non-complementary sequence (NC). This decrease is attributed to the specific hybridization between the immobilized DNA probe and HIVc, thereby confirming the biosensor's selectivity towards HIV. Comparing the percentage signal decrease recorded for the different probe immobilization times, the most significant signal difference before and after hybridization with the HIVc sequence occurs with a 24-h immobilization time. Therefore, this was selected as the optimal time for developing the DNA biosensor, CSPE/FLB/HIV-SH.

Comparing the percentages of electrochemical signal decrease recorded for Dend$_{VIH}$-SH (Fig. 3D) with those of the 24-h DNA probe (Fig. S4, orange bar), it can be observed, as expected, that recognition is better for the Dend$_{VIH}$-SH. The signal decrease recorded is 20 % higher and more reproducible since the DNA dendrimer structure has a higher number of hybridization sites, allowing for signal amplification compared to the DNA probe.

These results demonstrate that using the HIV-based DNA dendrimer as the biorecognition element allows for signal amplification and reduces the preparation time of the biosensing platform.

After optimizing all steps in the HIV dendrimer-based DNA biosensor development and testing its capacity to detect the specific HIV sequence, the response of the CSPE/FLB/Dend$_{VIH}$-SH biosensing platform was studied for different concentrations of the HIV DNA sequence under previously established optimal conditions. To this end, the biosensing platform was incubated with varying concentrations of the HIVc sequence, ranging from 10.0 fM to 100 pM. The resulting calibration plot, presented in Fig. 4A, depicts the normalized current intensity, calculated as the absolute value of the difference between the electrochemical signal recorded after and before (blank, i_B) the incubation with the target sequence, divided by i_B, plotted against the logarithm of the HIVc concentration. A linear correlation is observed, described by the equation: $|(i-i_B)/i_B| = 0.181 \cdot \log[HIVc] + 0.634$ ($R = 0.9903$). Each data

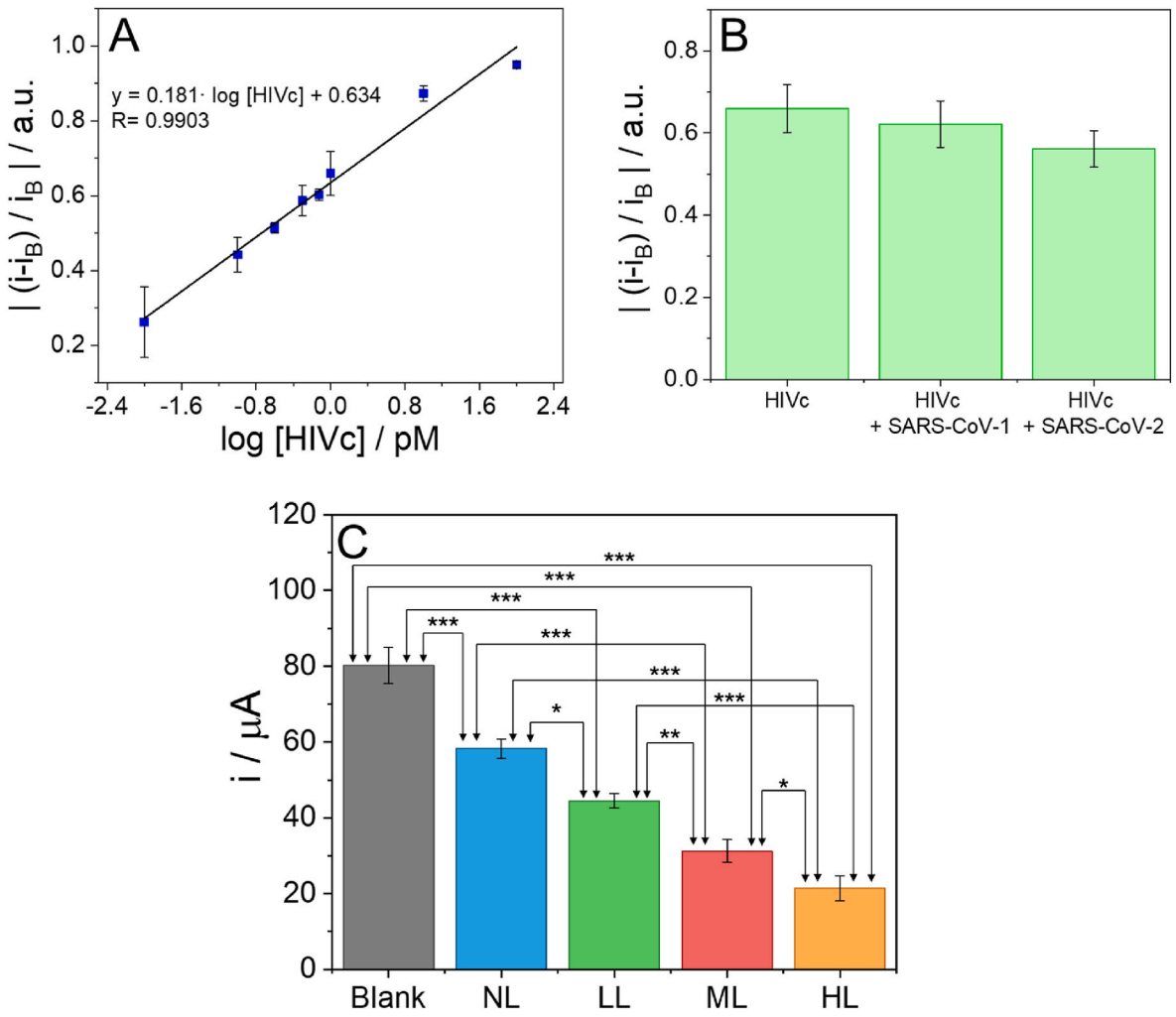

Fig. 4. Calibration plot (**A**) of the normalized current intensity plotted against the logarithm of the HIVc sequence concentration (from 10.0 fM to 10.0 pM). Column chart (**B**) of the normalized current intensity obtained for a 1.00 pM concentration of the HIVc sequence, both in absence and presence of potential interfering viral sequences (SARS-CoV-1 and SARS-CoV-2), each at the same concentration. Dendrimer-based DNA biosensor response to clinical plasma samples (**C**) from HIV patients with undetectable viral load (NL, blue bar), low viral load (LL, green bar), medium load (ML, red bar) and high load (HL, orange bar), and control signal (Blank, grey bar) recorded at the oxidation potential of Azure A. Statistical analysis was performed using one-way ANOVA followed by Tuckey's test (pairwise comparison), with the RConsole software. Significance codes: 0 '***' 0.001 '**' 0.01 '*' 0.05 '.' 0.1 ' ' 1. Data are present as mean ± SD (n = 3). (For interpretation of the references to colour in this figure legend, the reader is referred to the Web version of this article.)

represents the mean of three independent measurements, yielding a percentage coefficient of variation (CV%) of 5.94 % and a sensitivity of 0.181 a.u. log (pM^{-1}). The detection limit (LOD) was determined to be 3.03 fM, using the formula $y = X_B + 3{\cdot}S_B$ (where X_B is the mean of three times the electrochemical response of the blank and S_B the standard deviation), introducing the normalized current intensity response obtained in the calibration plot and calculating the concentration of HIV.

To demonstrate the improvements in sensitivity and amplification capacity of the HIV-based DNA dendrimer, a calibration was performed using the CSPE/FLB/HIV-SH platform (see Scheme S1 in the Supporting Information), for concentrations of the HIVc sequence ranging from 500 fM to 100 pM. Fig. S5 in the SI presents the calibration plot obtained for the normalized current intensity registered (calculated as previously described) versus the logarithm of the HIVc concentration. The linear equation describes the upward linear correlation observed: $|(i\text{-}i_B)/i_B| = 0.238{\cdot}\log[HIVc] + 0.218$ (R = 0.9944) (n = 3). These results yield a sensitivity of 0.238 a.u. log (pM^{-1}) and a CV of 2.27 %. The detection limit obtained was 0.235 pM (calculated using the equation $y = XB + 3{\cdot}S_B$, as explained previously). Comparing this with the LOD obtained for the HIV dendrimer-based DNA biosensor, it can be affirmed that the sensitivity of the device improves considerably, further demonstrating the benefits that the use of DNA dendrimers brings to biosensor design.

The selectivity of the dendrimer-based DNA biosensor was further evaluated through an interference study. The biosensor response was analyzed in solutions containing only the specific HIV sequence at a concentration of 1.00 pM, and in solutions containing the HIV sequence along with potentially interfering viral DNA sequences, such as SARS-CoV-1 and SARS-CoV-2, at the same concentration. As shown in Fig. 4B, the normalized biosensor response to HIVc remained virtually unchanged in the presence of these non-target genetic materials, as hybridization occurred exclusively with the HIVc sequence, totally complementary to the capture probe sequence located within the DNA dendrimer structure. These results confirm the high selectivity of the biosensor developed for the specific HIV DNA sequence.

The stability of the dendrimer-based DNA biosensor was assessed by measuring the response of a platform that, after being prepared and stored for 60 days at 4 °C, was exposed to a 1.00 pM HIVc sequence. The electrochemical response remains almost stable, changing by 23 % from the initial response.

3.4. HIV virus DNA sequence detection in human serum samples

To establish the matrix effect, we decided to test the developed platform using human serum samples. Details regarding the preparation of human serum samples spiked with 1.00 pM of the HIVc sequence, as well as the methodology used to calculate the normalized current intensity response, are provided in the experimental section of the SI. Calculating the differences between the non-dopped human serum sample electrochemical response with the blank, recalculating the electrochemical response obtained for three different measurements after the incubation of the CSPE/FLB/$Dend_{VIH}$-SH platform with the HIVc-dopped human serum sample and interpolating the normalized current intensity obtained for the 1.00 pM concentration of the HIVc sequence into the calibration plot, a recovery of (99 ± 8) % was obtained. With this result, it is possible to confirm that the HIV dendrimer-based DNA biosensor developed is capable of detecting HIV by its genetic code in human serum samples, and that it represents a potential alternative methodology for virus detection.

3.5. HIV DNA sequence detection in clinical plasma patient samples and statistical analysis

Finally, based on the excellent results obtained for the HIV dendrimer-based DNA biosensor, and the emerging need for new devices capable of early virus detection to curb the spread of diseases such as AIDS, especially in developing countries, we have taken a step further and tested the developed biosensor for detecting the HIV in infected patient samples. The biosensing platform developed was validated by studying the response of the dendrimer-based DNA biosensor to clinical plasma samples that had not undergone prior PCR amplification, from negative patients (NL, blue bar), or infected patients, that contains the specific HIV viral sequence in different viral loads, low viral load (LL, green bar), medium viral load (ML, red bar), and high viral load (HL, orange bar). The samples were supplied and previously analyzed by PCR using the Cobas 6800 automated system (Roche) by the "Microbiología y Parasitología Clínicas" service of the Hospital Universitario La Paz, with the consent of all participants and approved by "Comité de Ética de la Investigación con Medicamentos del Hospital Universitario La Paz". Reference: PI-6465. Three samples from each of the infected patient groups (LL, ML, and HL) and one negative sample (NL) as a control, were analyzed after pretreatment, as detailed in the experimental section in the SI. The signal recorded at the Azure A oxidation potential was compared with that of the biosensor before incubation (Blank, grey bar). The results obtained for one sample from each group, analyzed in triplicate, are shown in Fig. 4C. As can be observed, after incubation with the clinical samples, a decrease in current intensity was recorded, even for the negative sample, indicating that the effect of the matrix studied on the biosensor response should be considered. Comparing the signals for each of the samples from infected patients, it can be demonstrated that as the viral load of the sample increases, the current intensity decreases (resulting in a higher normalized signal compared to the blank). Statistical analyses confirm that the signals recorded for each of the samples are significantly different, with a significance level of 0, except between LL and ML, where the significance level is 0.001, and between NL and LL, and ML and HL, where it is 0.05. In addition, the biosensor response was compared for each of the three samples analyzed (in triplicate) within each of the different viral load groups, as shown in Fig. S6. Statistical analysis reveals that the recorded signals do not differ significantly between samples within each group. Only in the case of low viral load samples a difference was observed between LL1 and LL2 with a significance level of 0.001, and between LL2 and LL3 of 0.1. Based on the data, it can be concluded that the dendrimer-based DNA biosensor developed is capable of detecting HIV in plasma samples from infected individuals with varying viral loads (low, medium, or high), although it cannot distinguish between samples within the same group with significant accuracy.

Table S2 presents electrochemical biosensors described in the literature for detecting HIV. The analytical performance of the Dendrimer-based DNA biosensor developed in this work compares favourably with similar platforms reported in the literature, exhibiting an improved detection limit and highlighting the signal amplification capabilities provided by the DNA dendrimer. This proves the great applicability of the biosensing platform for HIV detection.

4. Conclusions

This work demonstrates that the integration of nanomaterials such as FLB and nanostructures like DNA dendrimers enables the development of highly sensitive DNA biosensors. Specifically, a dendrimer-based DNA biosensor was developed using FLB as an anchoring platform for the immobilization of the thiolated HIV-based DNA dendrimer synthesized onto the surface of the transducer (CSPE). The DNA dendrimer served as a biorecognition element for the sensitive and selective detection of HIV genetic code. Electrochemical detection of the hybridization event was achieved via Differential Pulse Voltammetry (DPV), using Azure A (AA) as a redox indicator, due to its affinity for DNA. The developed HIV-based DNA biosensor was incubated with concentrations from 10.0 fM to 10.0 pM, and exhibited a detection limit of 3.03 fM, a value lower than those reported for similar platforms. Its selectivity was confirmed by the absence of significant signal interferences from non-complementary sequences and other viral DNAs. The biosensor maintained stable performance over a 60-day storage period. Analytical validation was carried out using human serum samples dopped with HIVc at 1.00 pM, achieving a recovery rate of 99 %. Furthermore, the biosensor successfully detected HIV in clinical plasma samples from patients with varying viral loads, without prior PCR amplification. These results position the dendrimer-based DNA biosensor as a promising alternative to conventional virus detection methodologies.

CRediT authorship contribution statement

Estefanía Enebral Romero: Writing – review & editing, Writing – original draft, Methodology, Investigation, Formal analysis, Data curation. **Marta Toldos-Torres:** Methodology, Investigation. **David López-Diego:** Writing – review & editing, Methodology, Investigation, Formal analysis, Data curation. **Mónica Luna:** Writing – review & editing, Supervision, Resources, Project administration, Funding acquisition. **Marta Failde:** Methodology, Investigation, Formal analysis. **Brais González-Tobío:** Writing – review & editing, Methodology, Investigation, Formal analysis, Data curation. **Félix Zamora:** Writing – review & editing, Supervision, Resources, Project administration, Funding acquisition. **Iker Falces-Romero:** Methodology, Investigation, Formal analysis, Data curation. **María Luisa Montes:** Methodology, Investigation, Formal analysis, Data curation. **Tania García-Mendiola:** Writing – review & editing, Writing – original draft, Supervision, Resources, Project administration, Funding acquisition, Formal analysis, Data curation, Conceptualization.

Declaration of competing interest

The authors declare that they have no known competing financial interests or personal relationships that could have appeared to influence the work reported in this paper.

Acknowledgements

This work was financially supported by the Spanish Ministry of Science, Innovation and Universities through the following projects: MCIU-25-RED2024-153970-T, PID2023-150844OB-I00, RED2022-134120-T, PID2022-138908NB-C31, PDC2021-120782-C21, and TED2021-129738B-I00. Estefanía Enebral-Romero acknowledges funding from the project "Nanotecnología para detección del SARS-CoV-2 y

sus variantes (NANOCOV)" and a predoctoral research contract supported by grant CEX2020-001039-S, funded by MCIN/AEI/10.13039/501100011033.

F.Z. acknowledges support from Spanish Ministry of Science, Innovation and Universities with the grant PID2022-138908NB-C31, from the Community of Madrid, the European Union's NextGenerationEU programme and the Recovery, Transformation and Resilience Plan, with the "MAD2D-CM-UAM" project, and from the Spanish Ministry of Science and Innovation through the "María de Maeztu" Programme for Units of Excellence in R&D (CEX2023-001316-M). B. G. acknowledges the financial support from the "Ayuda para Contratos Predoctorales para la Formación de Doctores" program of MICINN (PRE2020-093162). Additional support was provided by the European Innovation Council under grant agreement 101047081 (EVA).

We also acknowledge the MiNa Laboratory at IMN for technical support, and funding from the MCIN/AEI/10.13039/501100011033, EU (FEDER, FSE), and Next Generation EU/PRTR (EQC2021-006944-P). Special thanks are extended to Iker Falces and María Luisa Montes from Hospital Universitario La Paz for their collaboration in providing clinical plasma samples from HIV patients.

Appendix A. Supplementary data

Supplementary data to this article can be found online at https://doi.org/10.1016/j.bios.2025.118014.

Data availability

Data will be made available on request.

References

Abrego-Martinez, J.C., Jafari, M., Chergui, S., Pavel, C., Che, D., Siaj, M., 2022. Biosens. Bioelectron. 195, 113595.

Afonso, A.S., Pérez-López, B., Faria, R.C., Mattoso, L.H.C., Hernández-Herrero, M., Roig-Sagués, A.X., Maltez-da Costa, M., Merkoçi, A., 2013. Biosens. Bioelectron. 40, 121–126. https://doi.org/10.1016/j.bios.2012.06.054.

Bai, T., Wei, B., 2019. Nanoscale 11, 23105–23109. https://doi.org/10.1039/C9NR07196B.

Baig, N., 2023. Composites Part A: Applied Science and Manufacturing, vol. 165, 107362. https://doi.org/10.1016/j.compositesa.2022.107362.

Enebral-Romero, E., García-Fernández, D., Gutiérrez-Gálvez, L., López-Diego, D., Luna, M., García-Martín, A., Salagre, E., Michel, E.G., Torres, Í., Zamora, F., García-Mendiola, T., Lorenzo, E., 2024. Biosens. Bioelectron. 261, 116500. https://doi.org/10.1016/j.bios.2024.116500.

Farzin, L., Shamsipur, M., Samandari, L., Sheibani, S., 2020. Talanta 206, 120201. https://doi.org/10.1016/j.talanta.2019.120201.

Gutiérrez-Gálvez, L., García-Fernández, D., Barrio, M.D., Luna, M., Torres, Í., Zamora, F., Navío, C., Milán-Rois, P., Castellanos, M., Abreu, M., Cantón, R., Galán, J.C., Somoza, Á., Miranda, R., García-Mendiola, T., Lorenzo, E., 2024. Talanta 269, 125405. https://doi.org/10.1016/j.talanta.2023.125405.

Kabiibi, F., Tamukong, R., Muyindike, W., Yadesa, T., 2024. HIV Volume 16, 95–107. https://doi.org/10.2147/HIV.S449947.

Liébana, S., Brandão, D., Cortés, P., Campoy, S., Alegret, S., Pividori, M.I., 2016. Anal. Chim. Acta 904, 1–9. https://doi.org/10.1016/j.aca.2015.09.044.

Liu, L., Han, L., Wu, Q., Sun, Y., Li, K., Liu, Y., Liu, H., Luo, E., 2021. J. Mater. Chem. B 9, 4991–5007. https://doi.org/10.1039/D1TB00689D.

Martínez-Periñán, E., García-Mendiola, T., Enebral-Romero, E., Del Caño, R., Vera-Hidalgo, M., Vázquez Sulleiro, M., Navío, C., Pariente, F., Pérez, E.M., Lorenzo, E., 2021. Biosens. Bioelectron. 189, 113375. https://doi.org/10.1016/j.bios.2021.113375.

Meng, H.-M., Zhang, X., Lv, Y., Zhao, Z., Wang, N.-N., Fu, T., Fan, H., Liang, H., Qiu, L., Zhu, G., Tan, W., 2014. ACS Nano 8, 6171–6181. https://doi.org/10.1021/nn5015962.

Mohri, K., Kusuki, E., Ohtsuki, S., Takahashi, N., Endo, M., Hidaka, K., Sugiyama, H., Takahashi, Y., Takakura, Y., Nishikawa, M., 2015. Biomacromolecules 16, 1095–1101. https://doi.org/10.1021/bm501731f.

Mohri, K., Nishikawa, M., Takahashi, N., Shiomi, T., Matsuoka, N., Ogawa, K., Endo, M., Hidaka, K., Sugiyama, H., Takahashi, Y., Takakura, Y., 2012. ACS Nano 6, 5931–5940. https://doi.org/10.1021/nn300727j.

Qian, H., Guo, X., Yang, H., Bao, T., Wu, Z., Wen, W., Zhang, X., Wang, S., 2024. Biosens. Bioelectron. 261, 116522. https://doi.org/10.1016/j.bios.2024.116522.

Rizvi, A.S., Murtaza, G., Zhang, W., Xue, M., Qiu, L., Meng, Z., 2023. J. Pharmaceut. Biomed. Anal. 227, 115104. https://doi.org/10.1016/j.jpba.2022.115104.

Rohaizad, N., Mayorga-Martinez, C.C., Fojtů, M., Latiff, N.M., Pumera, M., 2021. Chem. Soc. Rev. 50, 619–657. https://doi.org/10.1039/D0CS00150C.

Su, S., Sun, Q., Gu, X., Xu, Y., Shen, J., Zhu, D., Chao, J., Fan, C., Wang, L., 2019. TrAC, Trends Anal. Chem. 119, 115610. https://doi.org/10.1016/j.trac.2019.07.021.

Tian, R., Ma, W., Wang, Lue, Xie, W., Wang, Y., Yin, Y., Weng, T., He, S., Fang, S., Liang, L., Wang, Liang, Wang, D., Bai, J., 2024. Bioelectrochemistry 157, 108651. https://doi.org/10.1016/j.bioelechem.2024.108651.

Torres, I., Villa-Manso, A.M., Revenga-Parra, M., Gutiérrez-Sánchez, C., Aldave, D.A., Salagre, E., Michel, E.G., Varela, M., Gómez-Herrero, J., Lorenzo, E., Pariente, F., Zamora, F., 2022. Applied Materials Today 26, 101360. https://doi.org/10.1016/j.apmt.2021.101360.

Xu, J., Zhao, W., Lai, Y., Li, H., Zhang, S., Yu, R., 2025. Biosens. Bioelectron. 272, 117111. https://doi.org/10.1016/j.bios.2024.117111.

Yang, H., Xu, Y., Hou, Q., Xu, Q., Ding, C., 2022. Biosens. Bioelectron. 208, 114216. https://doi.org/10.1016/j.bios.2022.114216.

Ye, T., Xu, Y., Chen, H., Yuan, M., Cao, H., Hao, L., Wu, X., Yin, F., Xu, F., 2024. Biosens. Bioelectron. 251, 116127. https://doi.org/10.1016/j.bios.2024.116127.

Zhao, H., Lv, J., Li, F., Zhang, Z., Zhang, C., Gu, Z., Yang, D., 2021. Biomaterials 268, 120591. https://doi.org/10.1016/j.biomaterials.2020.120591.

Zhou, T., Wang, Y., Dong, Y., Chen, C., Liu, D., Yang, Z., 2014. Bioorg. Med. Chem. 22, 4391–4394. https://doi.org/10.1016/j.bmc.2014.05.062.